Entropic stress of grafted polymer chains in shear flow

View Online   Export Citation   CrossMark

Jan Mees,[1,2] 🆔 Thomas C. O'Connor,[3] 🆔 and Lars Pastewka[1,2,a] 🆔

AFFILIATIONS

[1] Department of Microsystems Engineering, University of Freiburg, Georges-Köhler-Allee 103, Freiburg 79110, Germany
[2] Cluster of Excellence LivMatS, Freiburg Center for Interactive Materials and Bioinspired Technologies, University of Freiburg, Georges-Köhler-Allee 105, Freiburg 79110, Germany
[3] Department of Materials Science and Engineering, Carnegie Mellon University, Pittsburgh, Pennsylvania 15213, USA

Note: This paper is part of the JCP Special Topic on Adhesion and Friction.
[a] Author to whom correspondence should be addressed: lars.pastewka@imtek.uni-freiburg.de

ABSTRACT

We analyze the shear response of grafted polymer chains in shear flow via coarse-grained molecular dynamics simulations with an explicit solvent. We find that the solvent flow penetrates into almost the whole brush for "mushroom"-type brushes but only a few bond distances for dense brushes. In all cases, the external stress on the wall equals the entropic stress associated with the distorted polymer conformations. We find that the external stress increases linearly with shear rate at low rates and sublinearly at high rates. The transition from linear to sublinear scaling occurs where chains react to flow by reorienting. Sublinear scaling with shear rate disappears if the shear rate is nondimensionalized with the effective relaxation time of chain subsegments located in the outer part of the brush that experiences flow.

17 January 2024 10:27:11

I. INTRODUCTION

Polymer brushes are systems of surface-grafted polymer chains. They have been used in various applications, such as stabilizing colloidal suspensions,[1–3] anti-fouling coatings,[4,5] and adjusting surface interactions and wetting behavior.[6] They naturally occur on the interface of complex biological or bio-inspired systems, such as cartilage[7] or hydrogels,[8–17] and are known for their excellent lubricating properties.[18–20]

In this paper, we apply molecular simulations to study the relation between interfacial shear stress and polymer conformation in brushes exposed to solvent flow. We model systems of grafted chains with varying chain length and grafting density [see Figs. 1(a) and 1(b)] and analyze their microscopic response to shear flow. We explore the polymer's role by computing the contribution of the conformational entropy to the shear stress in the nonequilibrium chain-conformations imposed by the external flow.[21,22]

Prior simulation studies on grafted polymer chains discussed polymer conformations during flow,[23–29] but those studies did not discuss mechanical stresses in the system and focused on high

grafting density. Here, we explicitly analyze stresses with the goal to connect polymer conformation to external drivers, as in frictional contacts. We also include brushes with low grafting density, such as those encountered on the surfaces of hydrogels,[15–17] in the hope that our work contributes to the ongoing debate on the roles of solvent hydrodynamics and nonequilibrium polymer conformations in the tribology of those systems.[10–17] Our work is hence most representative of a sliding polymeric system in a hydrodynamic regime.

Equilibrium chain conformations depend on grafting density. At low grafting densities, in what is called the "mushroom" regime, the chains do not interact with each other. With increasing grafting density Γ, the chains start to overlap and adopt increasingly straight, brush-like conformations due to excluded volume effects.[19] The transition between both regimes occurs at $\Gamma \approx \Gamma^*$, with $\Gamma^* = 1/(\pi R_g^2)$, where R_g is the radius of gyration of the individual chain inside the brush.

When exposed to shear flow, the solvent's velocity gradient penetrates a certain distance into the brush before it is screened out.[30] This momentum transport into the brush reorients and elon-
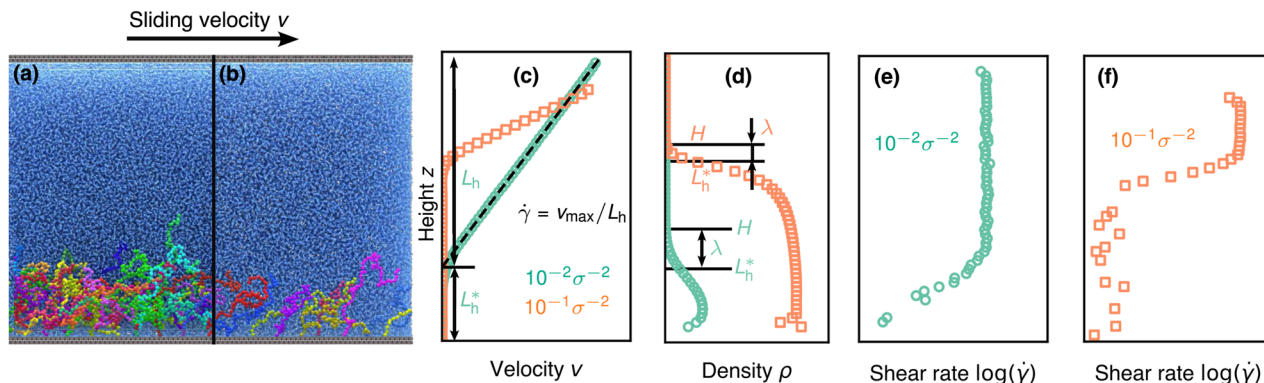
FIG. 1. (a) Polymer chains with 60 beads/chain and grafting density $\Gamma = 10^{-2}\,\sigma^{-2}$ at sliding speed $v = 5 \times 10^{-2}\,\sigma\tau^{-1}$. (b) Only two rows of grafted chains are depicted for clarity. Each chain has a different color to ease visibility. (c) The solvent's velocity profile in the shear direction is used to determine the effective shear rate $\dot\gamma$, here shown for a system with $N = 60$ beads/chain at grafting densities $\Gamma = 10^{-2}\,\sigma^{-2}$ (green) and $10^{-1}\,\sigma^{-2}$ (orange). The dashed lines represent the fits. (d) Polymer density distribution as a function of height for the same systems. The hydrodynamic-penetration length λ is determined as the difference of brush height H and L_{h}^{*}. (e) and (f) show the height dependency of the local shear rate $\dot\gamma(z) = \Delta v/\Delta z$.

gates chains in the direction of shear.[23–29] As a result, a grafted polymer chain in shear flow is subject to three forces: an osmotic force due to the gradient in polymer concentration across the interface, a shear force due to the solvent's shear flow, and a restoring force due to conformational entropy.[31] Studies have shown that the competition between these forces in nonlinear flows can drive chains to split into two coexisting populations, with one population elongating in flow, while the other remains unperturbed within the brush.[29,32–34]

Several theoretical models have been proposed for polymer brushes exposed to shear flow.[31–33,35–37] The model in a study by Clément *et al.*[33] builds on the fact that shear flow only penetrates over the hydrodynamic-penetration length λ into the brush. The system's steady-state shear response is determined by the competition between the shear rate $\dot\gamma$ and the relaxation time τ_{r} of the chains' outermost "blobs" of size ξ. Assuming that within each blob, the chain segments follow Zimm dynamics,[32,33,37] the relaxation time is given by[38]

$$\tau_{\mathrm{r}} \approx \eta_{\mathrm{s}}\xi^{3}/k_{\mathrm{B}}T, \qquad (1)$$

where ξ^{3} is the correlation volume and η_{s} is the solvent viscosity. For a single chain in a good solvent, ξ is the radius of gyration R_{g} of the chain.[21] It is often implicitly assumed[33,37] that the size of the outermost blob that reacts to shear flow corresponds to the hydrodynamic-penetration length, i.e., $\xi \sim \lambda$. If this is the case, then the system's response can be characterized by the Weissenberg number Wi $= \dot\gamma\tau_{\mathrm{r}}$ with τ_{r} obtained from Eq. (1) for a blob size that is proportional to λ.

Experiments commonly do not have access to λ and, therefore, τ_{r}. The Weissenberg number Wi$^{*} = \dot\gamma\tau_{\mathrm{r}}^{*}$ is then defined with respect to the equilibrium relaxation time of the full free chain, τ_{r}^{*}.[11,12,39–41] The key question that we are trying to answer is what the consequences of this approximation are for the observation of macroscopic properties, in particular the shear stress. Our results confirm that only the part of the brush with height λ actually exposed to solvent shear determines the brush's shear response. The value of

λ varies with shear rate and grafting density, information that is not experimentally accessible. This implies that the rate-dependence of macroscopic properties, such as the external stress, will depend on how Wi is defined. In the regime where chains elongate, the external stress appears to depend sublinearly on Wi only if a shear-rate-independent relaxation time, such as an equilibrium relaxation time, is used to compute the Weissenberg number, as is typical for experiments measuring friction in self-mated hydrogels and polymer brushes.[11,12,39,41]

II. THEORY

The stress in a polymer solution is comprised of contributions from the solvent's viscous dissipation, hydrostatic pressure, and polymer entropy. The stress tensor is often modeled as[21]

$$\sigma_{\alpha\beta} = \eta_{\mathrm{s}}(\kappa_{\alpha\beta} + \kappa_{\beta\alpha}) - p\delta_{\alpha\beta} + \frac{\rho}{n}\langle f_{\alpha}r_{\beta}\rangle, \qquad (2)$$

where α and β denote the Cartesian coordinates. The solvent's viscous dissipation yields a contribution $\eta_{\mathrm{s}}(\kappa_{\alpha\beta} + \kappa_{\beta\alpha})$, where $\kappa_{\alpha\beta}$ is the local shear rate. The hydrostatic pressure's contribution is $-p\delta_{\alpha\beta}$, with pressure p and Kronecker delta $\delta_{\alpha\beta}$. $\langle\cdot\rangle$ represents the ensemble average. Finally, the polymer's contribution to the stress tensor is

$$\sigma_{\alpha\beta}^{\mathrm{entr}} = \rho\langle f_{\alpha}r_{\beta}\rangle/n, \qquad (3)$$

where ρ is the polymer's number density and n is the number of bonds per chain. The force $\vec{f}$ is the sum of non-hydrodynamic forces acting on a given chain, and $\vec{r}$ is the chain's end-to-end distance vector.

We can now insert into Eq. (3) the equation for the non-linear, entropic force of a freely jointed polymer chain $|\vec{f}| = k_{\mathrm{B}}T\,\mathcal{L}^{-1}(h)/l_{\mathrm{k}}$,[22] in which l_{k} is the Kuhn length, $\mathcal{L}^{-1}$ is the inverse Langevin function,[38] and $h = |\vec{r}|/nb$ is the extension ratio with a bond length b. The extension ratio is proportional to $n^{-1/2}$ for an ideal, Gaussian chain and unity for a fully extended chain. The Kuhn

length is defined as $l_k = C_\infty b$, in which C_∞ is Flory's characteristic ratio. We note that this is an approximation for the systems that we are studying, as it assumes that each chain is under uniform tension which is not the case in most real environments. However, past simulation work has shown that this approximation works well (see, for example, Ref. 22).

From Eq. (3), we obtain

$$\sigma_{\alpha\beta}^{\text{entr}} = \frac{\rho(\dot{\gamma})k_B T}{C_\infty} \langle \mathcal{L}^{-1}(h) h \; \hat{r}_\alpha \hat{r}_\beta \rangle, \tag{4}$$

where $\hat{r}_\alpha$ are the components of the unit vector $\vec{r}/r$ of the end-to-end distance. Flory's characteristic ratio is $C_\infty = 1.7$ for our system (see the Appendix for further details). The number density is given by $\rho = N_m/V$, where N_m is the number of monomers and $V = L_x L_y H(\dot{\gamma})$ is the volume occupied by the grafted chains, with H being the brush's height. The number density is shear rate-dependent because at higher shear rates, the chains tilt and stretch, changing the volume.

This derivation ignores changes to the chain's internal energy that might arise at large extensions and, hence, only captures the effects of changes in configurational entropy, which is usually the dominant source of stress in shearing flows. For the purpose of clarity and brevity, we henceforth call the polymer's contribution to the stress tensor the entropic stress $\sigma_{\alpha\beta}^{\text{entr}}$. Two different molecular effects go into the entropic stress. First, the hardening factor $\mathcal{L}^{-1}(h)h$ captures the mechanical effect of chain elongation. Second, the orientation factor $\hat{r}_\alpha \hat{r}_\beta$ captures the alignment of polymer chains.

III. METHODS

Our molecular system, depicted in Figs. 1(a) and 1(b), consists of polymer chains bonded to a face-centered cubic wall with a lattice spacing of $1.2\,\sigma$ and the [111] crystallographic direction facing the interface. The chains are bonded to the exposed wall beads following a hexagonal pattern with grafting density Γ. The polymers are described by a coarse-grained bead-spring model[42] in which the excluded volume is modeled by a Lennard-Jones (LJ) potential with interaction energy $\varepsilon = 1.0$, length $\sigma = 1.0$, and cutoff radius $r_{\text{cut}} = 1.6\,\sigma$. The masses are set to unity so that the time scale of the simulation is given by $\tau = \sigma(m/\varepsilon)^{1/2}$. Consecutive monomers (polymer beads) are connected by a nonlinear FENE bond with spring constant $k = 30.0\,\varepsilon\sigma^{-2}$ and maximum extension $R_0 = 1.5\,\sigma$.[42,43] The cutoff radius of the LJ interaction of bonded monomers is set to $r_{\text{cut}} = 2^{1/6}\,\sigma$, making the LJ interaction purely repulsive. The monomers interact with wall beads via an LJ interaction with $\varepsilon = 0.6$, $\sigma = 1.3$, and $r_{\text{cut}} = 1.6\,\sigma$. The monomers are bonded to the bottom wall via FENE bonds with spring constant $k = 30.0\,\varepsilon\sigma^{-2}$ and maximum extension $R_0 = 2.1\,\sigma$. The LJ interaction energy between the first bead near the wall and the wall is $\varepsilon = 0.8$ with length $\sigma = 1.5$ and cutoff radius $r_{\text{cut}} = 2^{1/6}\,\sigma$. The top wall does not interact with the polymer chains and only serves to impose a shear flow on the solvent.

We explicitly model a dimer solvent made of chains of length $N = 2$.[44,45] This type of explicit solvent inhibits layering effects at the walls and permits a larger time step than a monomer solvent.[39] The dimers are connected by FENE bonds with $k = 30.0\,\varepsilon\sigma^{-2}$ and maximum extension $R_0 = 1.3\,\sigma$. The LJ parameters are $\varepsilon = 0.8$, $\sigma = 0.8$,

and $r_{\text{cut}} = 2^{1/6}\,\sigma$. The non-bonded dimers interact via an LJ potential with parameters $\varepsilon = 0.5$, $\sigma = 1.0$, and $r_{\text{cut}} = 2.5\,\sigma$. The parameters for dimer–polymer interactions are set to $\varepsilon = 1.2$, $\sigma = 1.0$, and $r_{\text{cut}} = 2.5\,\sigma$. Finally, the dimers interact with the wall with $\varepsilon = 0.6$, $\sigma = 1.0$, and $r_{\text{cut}} = 2.5\,\sigma$. The aforementioned parameters are identical to the parameters used in a study by de Beer and Müser[46] to induce good-solvent conditions. The combined polymer and solvent system is simulated at a fixed surface concentration of 0.8 beads σ^{-3}. A downward pressure of $5 \times 10^{-4} m\sigma^{-1}\tau^{-2}$ acts on the top wall (which has no grafted polymer chains), slightly compressing the system. A representative system has the dimensions $L_x = 100\,\sigma$, $L_y = 87\,\sigma$, and $L_z = 64\,\sigma$ and contains 465 632 beads.

We use a DPD thermostat with friction coefficient $\gamma = 5m\tau^{-1}$ and cutoff $r_c = 2^{1/6}\,\sigma$ to thermalize the solvent and the polymers to a temperature of $k_B T = 0.6\,\varepsilon$,[47,48] where k_B is the Boltzmann constant. The top wall is moved at constant sliding speed v along the x axis in order to induce a shear flow in the solvent. We use a time step of $\Delta t = 5 \times 10^{-3}\,\tau$ in our simulations.

IV. RESULTS

A. Hydrodynamic penetration

We start by analyzing the penetration of solvent flow into the polymer brush. Between the brush and outer wall [see Fig. 1(c)], we find an ideal Couette flow with a velocity profile of the solvent that is linear in channel position. The solvent is sheared at a rate $\dot{\gamma} = v/L_h$, where L_h is the height of the solvent's Couette region. Note that for the definition of L_h, we extrapolate the linear Couette region into the brush toward the point where the velocity becomes zero. We use two different approaches to compute $\dot{\gamma}$ and L_h: while we determine $\dot{\gamma}$ from our simulations directly at high velocities, the shear rates obtained at low sliding velocities are dominated by thermal fluctuations. For sliding speeds $v < v'$, we compute $\dot{\gamma}$ by assuming that L_h does not change from its value at $v' = 5 \times 10^{-3}\,\sigma\tau^{-1}$.

Within the brush, hydrodynamic interactions are screened by the polymer chains—in other words, the flow velocity of the solvent vanishes inside the bulk of the brush. Given the overall simulation cell of height $L_h + L_h^*$ [see Fig. 1(c)], we obtain L_h^* as the height of the quiescent part of the brush. Comparing the quiescent height L_h^* with the actual height H of the brush yields the hydrodynamic-penetration length $\lambda = H - L_h^*$. We compute the brush height H from the position at which the density has decayed to 1% of its maximum value [see Fig. 1(d) and Ref. 49].

The influence of the grafting density on hydrodynamic penetration can be qualitatively observed in the logarithmic depiction of the shear rate [Figs. 1(e) and 1(f)]. For systems with $N = 60$ beads/chain, the grafting density at which the chains begin to overlap is $\Gamma^* = 1/(\pi R_g^2) \approx 9 \cdot 10^{-3}\,\sigma^{-2}$. For $\Gamma = 10^{-2}\sigma^{-2} \approx \Gamma^*$, the shear rate gradually increases to its maximum value in the Couette region, while the transition is much sharper for the denser system with $\Gamma = 10^{-1}\,\sigma^{-2} > \Gamma^*$.

For a more quantitative analysis, we plot in Fig. 2(a) the hydrodynamic-penetration length λ as a function of shear rate $\dot{\gamma}$ for three grafting densities Γ. While for our densest system, λ is independent of shear rate over the range of rates, λ decreases at high shear rates for semi-dilute and dilute systems. However, for
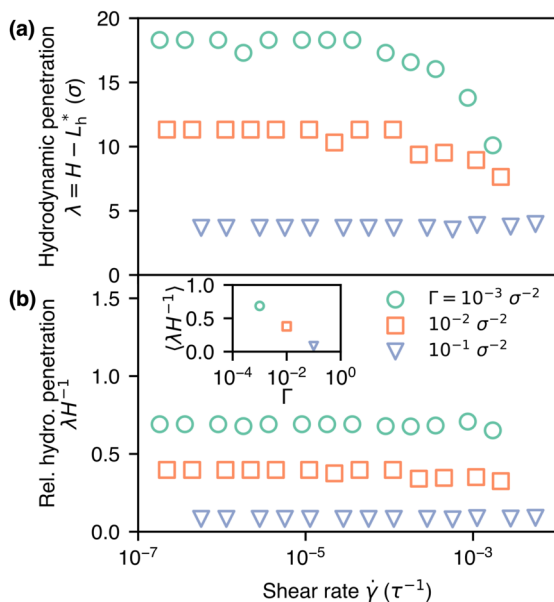
FIG. 2. (a) Hydrodynamic-penetration length λ as a function of shear rate $\dot\gamma$ for systems with 60 beads/chain and varying grafting density Γ. (b) λ normalized by the shear rate-dependent brush height H. The inset shows the average values as a function of grafting density.

all systems and shear rates, the hydrodynamic-penetration length λ is proportional to the brush height H. Figure 2(b) shows the normalized hydrodynamic-penetration length, λ/H. The dependence on shear rate disappears for λ/H, showing that the change in penetration length with shear rate of Fig. 2(a) is simply because the chains tilt and, hence, the brush shrinks at high shear rates. In other words, the number (or mass) of monomers in the region where shear flow penetrates is constant. For the lowest grafting densities with $\Gamma \ll \Gamma^*$, the solvent flow extends almost throughout the whole brush, while at $\Gamma \gg \Gamma^*$, the flow is unable to penetrate the brush significantly.

B. Shear stress

Solvent flow in our system is driven by a non-zero shear stress at the wall boundaries. Our simulation geometry consists of two parallel plates with an entrained molecular system and is mechanically extremely simple: Mechanical equilibrium means that the shear stress σ_{xz} is constant along the simulation cell's height (because $\partial \sigma_{xz}/\partial z = 0$). It follows that the external shear stress measured from the constraint forces of our rigid walls $\sigma_{xz}^{\text{wall}}$ is equal to the Newtonian viscous shear stress in the Couette-like region, $\sigma_{xz}^{\text{visc}} = \eta_s \dot\gamma$.

In the brush region, the shear stress will additionally contain a contribution from the polymer chains. In the simplest approximation (assuming independent chains), this will be the entropic stress in addition to the hydrodynamic, viscous stress of the solvent.[37] The entropic stress can be approximated from the individual chain conformations by Eq. (4). Note that Eq. (4) contains a volume average, which means it yields the mean entropic stress within the brush.

The solvent's hydrodynamic contribution to the shear stress is given by the solvent's average shear rate inside the brush,

$$\sigma_{xz}^{\text{hydro}} = \frac{\eta_s}{H} \int_0^H \mathrm{d}z \, \dot\gamma(z). \tag{5}$$

Figure 3 shows the entropic and hydrodynamic stresses obtained from these approximations alongside the measured wall stress. The results show that the entropic stress is approximately equal to the wall's shear stress for grafting densities $\Gamma = 10^{-2}\sigma^{-2}$ [Fig. 3(a)] and $\Gamma = 10^{-1}\sigma^{-2}$ [Fig. 3(b)]. In both cases, the hydrodynamic stress within the brush is much smaller than the entropic stress. The entropic stress of the polymer chains is the dominant contribution to the overall stress within the brush.

C. Dynamic response

The key parameter mediating the reaction of the brush to the shear flow is the local shear rate $\dot\gamma$ of the solvent rather than the sliding velocity v. The dynamic response of driven polymeric systems is, therefore, commonly nondimensionalized through the Weissenberg number $\text{Wi}^* = \dot\gamma\tau_r^*$, where τ_r^* is the equilibrium relaxation time of a single, dilute chain of length N. Examples include experiments and simulations in polymer brushes[39,40] or self-mated hydrogel friction.[11,12,41] The Weissenberg number compares an equilibrium measure (the relaxation time) with a non-equilibrium measure (the shear rate) and is proportional to $\dot\gamma$ as τ_r^* does not depend on shear rate.

We compute τ_r^* from independent molecular dynamics simulations of free chains via the time-autocorrelation function of the trace of the gyration tensor $\langle R_g(0)R_g(t)\rangle \propto \exp\left(-t/\tau_r^*\right)$.[21] We have confirmed that the relaxation time computed from Zimm dynamics[38] [see Eq. (1)] is close (within a factor of 2) to the relaxation time obtained from single-chain simulations. Figure 4 shows the entropic stress as a function of Wi^*. At low Wi^*, the shear stress increases linearly with Wi^*. This regime crosses over to a sublinear regime at high Wi^*.

We have pointed out already in the Introduction that the dynamics of the brush is controlled by an outmost blob of volume
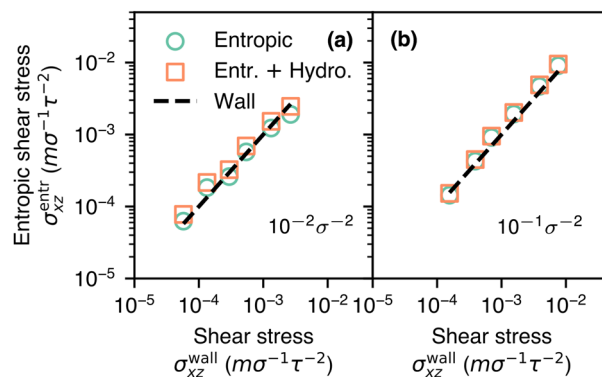

FIG. 3. Entropic and hydrodynamic shear stresses as a function of the wall's shear stress at grafting densities (a) $\Gamma = 10^{-2}\sigma^{-2}$ and (b) $\Gamma = 10^{-1}\sigma^{-2}$ for a system with 60 beads/chain. Each measurement corresponds to a different sliding velocity or shear rate. The dashed line represents the wall's shear stress.
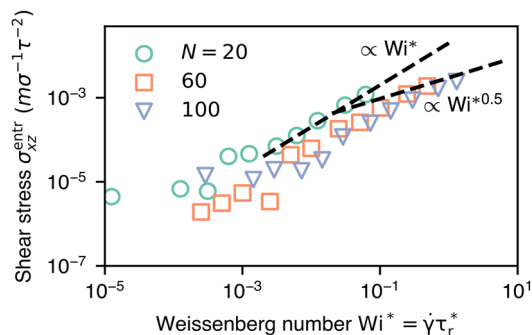
FIG. 4. Entropic shear stress as a function of equilibrium Weissenberg number Wi^* for different chain lengths N and a grafting density of $\Gamma = 10^{-2} \sigma^{-2}$, using the relaxation time τ_r^* of dilute chains of length N. The dashed lines are a guide to the eye.

ξ^3 rather than the dynamics of the full free chain; see, for example, Ref. 33. The relaxation time τ_r used in the definition of the Weissenberg number should, therefore, be the polymer relaxation time of this outermost blob, not the relaxation time τ_r^* of the free chain. While experiments typically have access to τ_r^* but not τ_r, we can compute τ_r from microscopic observations on our simulations. We assume that the individual blobs follow Zimm dynamics[38] and compute τ_r from the analytic expression Eq. (1). However, we do not know *a priori* the size ξ of the outermost blob. A crucial assumption of our model is, therefore, that ξ is proportional to the hydrodynamic-penetration length λ. In particular, we use $\xi = \lambda/\sqrt{6}$, since λ measures the penetration from the outermost part
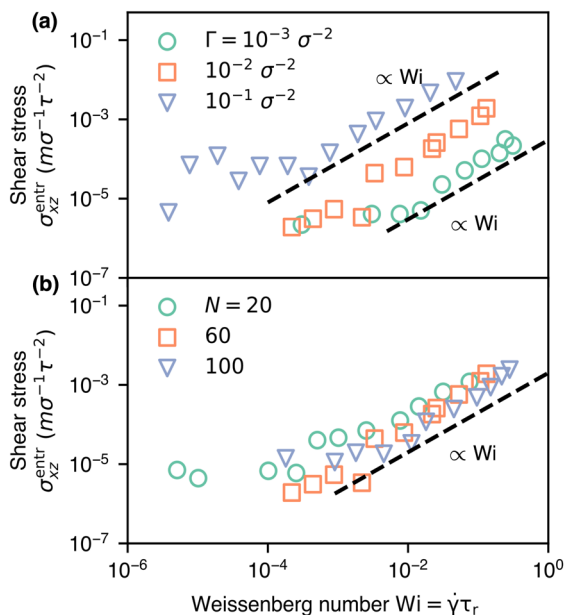

FIG. 5. (a) Entropic shear stress as a function of nonequilibrium Weissenberg number Wi at different grafting densities Γ for systems with 60 beads/chain. (b) Entropic shear stress as a function of Wi for different chain lengths at $\Gamma = 10^{-2} \sigma^{-2}$.

of the brush and corresponds to an end-to-end distance rather than a radius of gyration. Note that similar assumptions were made in early treatments of dense brushes.[33,37] Since λ changes with shear rate $\dot{\gamma}$, this implies that $\tau_r(\dot{\gamma})$ also depends on shear rate through Eq. (1). This nonequilibrium Weissenberg number $Wi = \dot{\gamma}\tau_r(\dot{\gamma})$ hence depends nonlinearly on $\dot{\gamma}$.

We now analyze the entropic shear stress as a function of the nonequilibrium Weissenberg number Wi. Figure 5(a) shows a linear dependence of the shear stress on Weissenberg number above $Wi \approx 0.01$. The linearity of the shear response exists independently of chain length, as evident from Fig. 5(b) that shows the entropic stress as a function of Wi for chains of different lengths at the same grafting density. Crucially, the sublinear scaling regime disappears when using the nonequilibrium Wi rather than the equilibrium Wi^* as the control parameter.

We note that the shear stress increases with grafting density, but the functional dependence of stress on Wi is independent of grafting density. Estimating the density for transition between mushroom and brushy regimes yields $\Gamma^* \approx 3.3 \times 10^{-2} \sigma^{-2}$ for $N = 20$ and $\Gamma^* \approx 4 \times 10^{-3} \sigma^{-2}$ for $N = 100$. This means that the short chains are in the mushroom regime, while the longer chains are brushy, yet both show a qualitatively identical rate-dependence of the stress response.

D. Chain conformation

We now relate the rate-dependent trends in stress to changes in the conformations of grafted chains. A common measure for conformation of a single chain is the gyration tensor,

$$R_{g,\alpha\beta}^2 = \frac{1}{N} \sum_i (x_{i,\alpha} - x_{CM,\alpha})(x_{i,\beta} - x_{CM,\beta}), \quad (6)$$

where $\vec{x}_i$ is the position of bead i and $\vec{x}_{CM}$ is the center of mass of the chain. Normalizing the gyration tensor in the direction of shear by its equilibrium value, we observe that the measurements collapse onto the same curve, despite changing grafting densities [Fig. 6(a)] or chain lengths [Fig. 6(b)]. In both cases, the gyration tensor in the direction of shear remains constant up to a threshold of $Wi = 1$, at which point it starts increasing rapidly. Note that the nonequilibrium Weissenberg number Wi seems to asymptotically approach a constant value for high shear rates because an increase in $\dot{\gamma}$ is compensated by a decrease in τ_r.

A more detailed view is offered by computing the orientation and hardening factors that comprise the entropic stress. In Figs. 6(c) and 6(e), we observe that the orientation factors fall onto the same curve, increasing linearly with Wi above approximately $Wi = 10^{-1}$. For the densest brush analyzed, the hardening factor is independent of Wi over the range analyzed. In contrast, our less dense systems show an increase in the hardening factor starting at approximately $Wi \approx 1$, consistent with the onset of chain elongation. Furthermore, their hardening factor is lower in the Wi-independent regime. When varying the chain length, we observe that the hardening factor increases with decreasing chain length in the Wi-independent regime. Furthermore, systems with longer chains show a stronger increase in the hardening factor at high Wi.

These trends are consistent with the expected conformations for flexible chains. At low grafting densities, the chains adopt random coil conformations with an equilibrium extension ratio
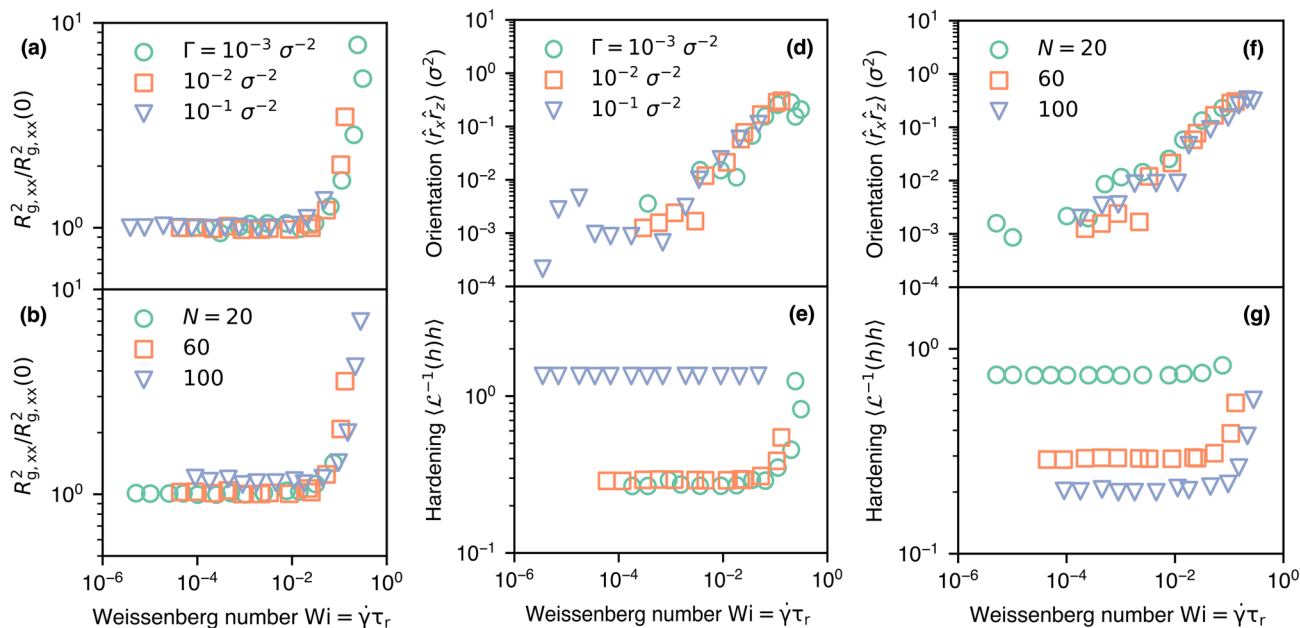
17 January 2024 10:27:11

FIG. 6. Normalized gyration tensor in the direction of shear as a function of Weissenberg number $\text{Wi} = \dot{\gamma}\tau_r(\dot{\gamma})$ for (a) different grafting densities Γ (with $N = 60$ beads/chain) and (b) different chain lengths N (with $\Gamma = 10^{-2}\sigma^{-2}$). Orientation and hardening factors for different grafting densities (c) and (d) and chain lengths (e) and (f).

$h \sim N^{-1/2}$ that decreases with increasing N. At higher grafting densities, the overlapping chains elongate, increasing both h and the hardening factor in equilibrium.

Finally, we investigate how chain conformation behaves as a function of distance to the wall. We do so by computing the

internal distance of chain subsegments with n_s bonds, normalized by the contour length $L_c = n_s b$ of the said segment. The segments are chosen such that the first bead is tethered to the wall. Figure 7 shows that for the lowest grafting density, the normalized end-to-end distance is reasonably close to results for a single, dilute chain at low Wi.
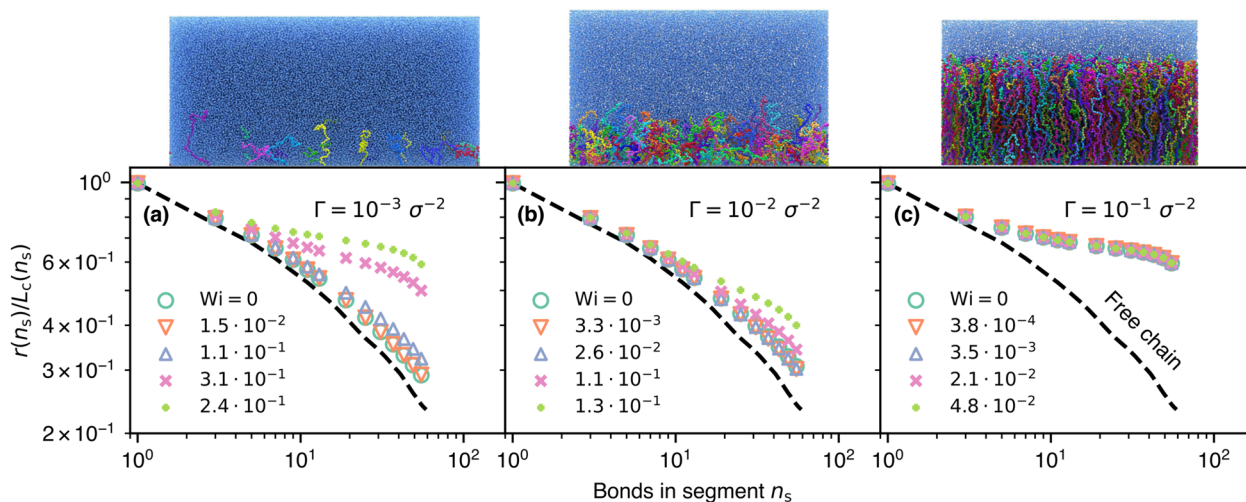

FIG. 7. Extension ratio $h(n_s) = r(n_s)/L_c(n_s)$ of chain segments with n_s bonds, starting from the grafting point. The extension ratio is the internal distance $r(n_s)$ normalized by the contour length $L_c = n_s b$ for systems at different Weissenberg numbers Wi. The individual polymers have $N = 60$ beads/chain. The panels (a), (b), and (c) show the results for different grafting densities Γ. The dashed lines represent the results for a free chain with $N = 60$ beads in dilute solutions. A representative snapshot of the system in equilibrium (Wi $= 0$) is depicted for each grafting density.

(The result for a dilute chain is shown by the dashed black lines in Fig. 7.) By comparison, as the grafting density increases, the normalized end-to-end distance in equilibrium deviates increasingly from the behavior of the single chain. At low Wi, the solvent flow does not affect chain conformations in all grafting densities analyzed. As Wi increases, the chains elongate significantly in both dilute and semi-dilute systems. While the flow's effect can be observed close to the wall for the dilute system, the point at which differences can be first noticed shifts further away from the wall (higher n_s) for the semi-dilute system. The dense system's morphology appears independent of Wi in the range analyzed.

V. DISCUSSION

The central observations from our simulations are as follows: The solvent flow penetrates into the brush up to a distance λ that increases with decreasing grafting density but is proportional to the rate-dependent brush-height, $\lambda \propto H(\dot{\gamma})$; the stress on the wall equals the entropic stress of the individual polymers, even at high grafting densities and high shear rates; the shear stress increases linearly with shear rate at low rates and sublinearly at high shear rates; and the shear stress increases linearly with the Weissenberg number Wi for all shear rates but only if the relaxation time that enters Wi is computed for the portion of the polymer chain penetrated by the shear flow.

We note that hydrodynamic penetration into brushes has widely been described in the literature (e.g., Ref. 30), and our results agree with those reports. Our observation $\lambda \propto H(\dot{\gamma})$ suggests that solvent screening is mediated by a roughly constant amount of polymer mass both in and out of equilibrium.

The implication of solvent flow, namely the transfer of momentum to the boundaries of the system, has, to the best of our knowledge, not been correlated with the microscopic morphology of the chains. It is noteworthy that the chain conformational entropy fully accounts for the external wall stress in all cases considered. This implies that even at low grafting densities, viscous solvent forces and intermolecular interactions contribute negligibly relative to the tension transmitted through chain backbones. This observation is consistent with the recent results on extensional stress in dense polymer melts, which can be related to conformation using the same freely jointed chain model.[22] The model even holds in highly nonequilibrium situations as encountered during extensional flow or at high shear rates.

At low shear rates, the stress increases linearly with shear rate as expected from linear response theory. However, we note that shear-rate independent regimes have been reported in simulations of brush[50] and hydrogel[41] friction. We do not observe such a rate-independent friction (also called Coulomb or adhesive friction) regime, which typically requires some form of elastic instability for its emergence.[51] While we cannot rule out that it exists, it is likely that Coulomb friction only emerges if the grafted chains can attach and detach from a counterbody,[52–56] which they cannot do in our case.

To quantify whether a shear-rate $\dot{\gamma}$ is "high" or "low," we need to compare it to a characteristic relaxation time of the polymers. The relevant time scale is the polymer relaxation time. Typically, the Weissenberg number is defined as Wi* = $\dot{\gamma}\tau_r^*$ using the equilibrium relaxation time of a free chain. Our simulations show a transition to a nonlinear increase in the shear stress with shear rate at Wi* ≈ 0.01. We point out that a similar sublinear behavior at high Wi* has been found in the friction coefficients of monodisperse brushes[39,40] and self-mated hydrogels,[10,11] with a transition also occurring near Wi* ≈ 0.01.[12,41] For self-mated hydrogels, this regime has been attributed to both non-equilibrium polymer effects[10] and hydrodynamic lubrication.[9] Our results indicate that the shear response of interfacial polymer chains might lie behind the observed frictional behavior of self-mated hydrogels.

The decomposition of the entropic stress into the orientation and hardening factors [Figs. 6(c)–6(f)] allows us to connect the shear response to morphological changes in the brush. At low shear rates, the brushes remain close to equilibrium and there is no clear signature in orientation and hardening factors. The chains reorient roughly at shear rates high enough that the stress starts to depend sublinearly on Wi*, which occurs at Wi* ≪ 1. Our simulations indicate that the process occurring at Wi* = 1 appears to be chain stretching, which can be directly seen in the hardening factors. The reason that we see chain stretching at this Weissenberg number is that the standard relaxation time, computed from the time-autocorrelation function of radius of gyration, corresponds to the slowest stretch relaxation time of the chain. Orientational relaxation typically occurs at longer time scales.[57]

In a polymer brush, the shear response should depend on the time scale of the relaxation τ_r of the brush's outermost boundary layer that is penetrated by the shear flow[33] and not the equilibrium relaxation time of the full chain τ_r^*. This length scale is the hydrodynamic-penetration length λ, which is independent of the shear rate for our densest system only [Fig. 2(a)]. As a result, it is valid to approximate the system's behavior with a constant relaxation time for a dense brush. However, for the semi-dilute and dilute systems, the hydrodynamic-penetration length and thereby the polymer relaxation time decrease significantly at high shear rates, which can be attributed to a decrease in the brush's height [Fig. 2(b)].

The relaxation time τ_r of the outmost part of the brush can be estimated from Zimm dynamics, Eq. (1), with a blob size $\xi \sim \lambda$. Using this (shear rate-dependent) relaxation time to compute the Weissenberg number, Wi = $\dot{\gamma}\tau_r(\dot{\gamma})$, we observe that the sublinear regime at high Wi* becomes linear. This behavior emerges at all grafting densities [Fig. 5(a)] and chain lengths [Fig. 5(b)]. These results are in agreement with the assumption made in previous theoretical models that polymer brushes in shear flow can be described as strings of Pincus blobs.[31,32,35,37,58]

Detailed morphological insights can be obtained from the conformations within the chain. The normalized internal distance (Fig. 7) becomes susceptible to shear flow closer to the wall in the dilute system than in the semi-dilute system. This can be attributed to the larger solvent flow within the chains in the dilute system, resulting in a larger hydrodynamic-penetration length. Our results show that chain conformations become increasingly linear due to the influence of the shear flow. The lack of Wi-dependency in the dense system can be attributed to the lack of shear flow penetration into the brush.

The normalized internal distance also sheds some light onto the relation between the orientation and hardening factors in dilute and semi-dilute systems. Even though in shear flow, the strongest shear force acting on the chains is located at the outermost blob, the reorientation of the chain involves the relaxation of the full chain.

However, in Fig. 7, we observe that chain elongation is not distributed equally among the chains' backbone but becomes stronger further away from the grafting site, i.e., it becomes stronger toward the location of the outermost blob.

VI. SUMMARY AND CONCLUSIONS

In summary, our results show that the brush's outermost "blob," the portion of the polymer chain that is exposed to shear of the solvent, determines the system's shear response. The flow penetrates less into dense than into dilute brushes. For dilute brushes, the flow penetrates less at high shear rates because the chains tilt. This leads to a shrinking, and effectively also a densification, of the brush. As a result, the relaxation time relevant to the system's shear response decreases at high shear rates. If this mechanism is not considered in the definition of the Weissenberg number—the quantity typically used to characterize the effect of solvent shear on polymeric systems—then the shear stress will appear to depend sublinearly on Wi. This phenomenology has been observed in polymer brush and self-mated hydrogel simulations and experiments at high Wi.[12,14,17,39–41]

AUTHOR DECLARATIONS

Conflict of Interest

The authors have no conflicts to disclose.

Author Contributions

Jan Mees: Conceptualization (equal); Data curation (equal); Investigation (equal); Methodology (equal); Software (equal); Writing – original draft (equal). **Thomas C. O'Connor**: Conceptualization (equal); Methodology (equal); Validation (equal); Writing – review & editing (equal). **Lars Pastewka**: Conceptualization (equal); Funding acquisition (equal); Methodology (equal); Supervision (equal); Validation (equal); Writing – review & editing (equal).

DATA AVAILABILITY

The data that support the findings of this study are available from the corresponding author upon reasonable request.

APPENDIX: FLORY'S CHARACTERISTIC RATIO

We compute Flory's characteristic ratio from polymer melt simulations with chains of length N. The systems were first equilibrated at a temperature of $T = 0.6\,\varepsilon$ and a pressure of
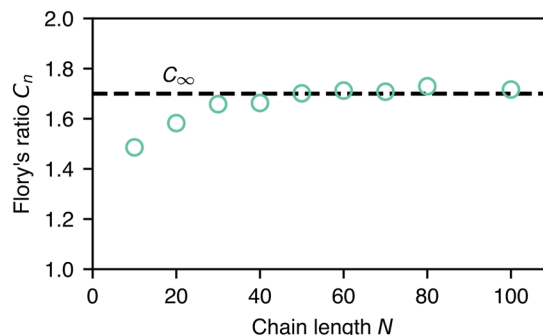

FIG. 8. Flory's characteristic ratio as a function of chain length. The dashed line represents $C_\infty = 1.7$.

$P = 5 \times 10^{-4}\, m\sigma^{-1}\tau^{-2}$. This procedure produced systems with a monomer density of approximately $\rho = 0.87\,\sigma^{-3}$. A second equilibration at constant volume followed at an increased temperature of $T = 2.0\,\varepsilon$ to increase diffusivity. Finally, at $T = 0.6\,\varepsilon$, the end-to-end distance of each chain was sampled every 10^3 time steps for 10^5 time steps. Flory's characteristic ratio was computed for each system using the relation $C_n = \langle R^2 \rangle / nb^2$, where $n = N - 1$ is the number of bonds in a chain.[38]

We see in Fig. 8 that Flory's ratio increases rapidly with N for $N < 30$ beads and saturates for higher N at ~1.7. It follows that $C_\infty = 1.7$.

REFERENCES

[1] D. H. Napper, *Polymeric Stabilization of Colloidal Dispersions* (Academic Press, 1983), Vol. 3.

[2] A. P. Gast and L. Leibler, "Interactions of sterically stabilized particles suspended in a polymer solution," Macromolecules **19**, 686 (1986).

[3] I. Borukhov and L. Leibler, "Stabilizing grafted colloids in a polymer melt: Favorable enthalpic interactions," Phys. Rev. E **62**, R41 (2000).

[4] A. Hucknall, A. J. Simnick, R. T. Hill, A. Chilkoti, A. Garcia, M. S. Johannes, R. L. Clark, S. Zauscher, and B. D. Ratner, "Versatile synthesis and micropatterning of nonfouling polymer brushes on the wafer scale," Biointerphases **4**, FA50 (2009).

[5] B. Xu, C. Feng, J. Hu, P. Shi, G. Gu, L. Wang, and X. Huang, "Spin-casting polymer brush films for stimuli-responsive and anti-fouling surfaces," ACS Appl. Mater. Interfaces **8**, 6685 (2016).

[6] P. Mansky, Y. Liu, E. Huang, T. Russell, and C. Hawker, "Controlling polymer-surface interactions with random copolymer brushes," Science **275**, 1458 (1997).

[7] G. Morgese, S. N. Ramakrishna, R. Simič, M. Zenobi-Wong, and E. M. Benetti, "Hairy and slippery polyoxazoline-based copolymers on model and cartilage surfaces," Biomacromolecules **19**, 680 (2018).

[8] J. P. Gong, "Friction and lubrication of hydrogels—Its richness and complexity," Soft Matter **2**, 544 (2006).

[9] A. C. Dunn, W. G. Sawyer, and T. E. Angelini, "Gemini interfaces in aqueous lubrication with hydrogels," Tribol. Lett. **54**, 59 (2014).

[10] A. Pitenis, J. Urueña, K. Schulze, R. Nixon, A. Dunn, B. Krick, W. Sawyer, and T. Angelini, "Polymer fluctuation lubrication in hydrogel gemini interfaces," Soft Matter **10**, 8955 (2014).

[11] J. M. Urueña, A. A. Pitenis, R. M. Nixon, K. D. Schulze, T. E. Angelini, and W. Gregory Sawyer, "Mesh size control of polymer fluctuation lubrication in gemini hydrogels," Biotribology **1–2**, 24 (2015).

[12] A. A. Pitenis and W. G. Sawyer, "Lubricity of high water content aqueous gels," Tribol. Lett. **66**, 113 (2018).

17 January 2024 10:27:11

[13] J. Mandal, R. Simič, and N. D. Spencer, "Impact of dispersity and hydrogen bonding on the lubricity of poly(acrylamide) brushes," Adv. Mater. Interfaces 6, 1900321 (2019).

[14] Y. A. Meier, K. Zhang, N. D. Spencer, and R. Simič, "Linking friction and surface properties of hydrogels molded against materials of different surface energies," Langmuir 35, 15805 (2019).

[15] N. Itagaki, D. Kawaguchi, Y. Oda, F. Nemoto, N. L. Yamada, T. Yamaguchi, and K. Tanaka, "Surface effect on frictional properties for thin hydrogel films of poly(vinyl ether)," Macromolecules 52, 9632 (2019).

[16] R. Simič, M. Yetkin, K. Zhang, and N. D. Spencer, "Importance of hydration and surface structure for friction of acrylamide hydrogels," Tribol. Lett. 68 64 (2020).

[17] W. Liu, R. Simič, Y. Liu, and N. D. Spencer, "Effect of contact geometry on the friction of acrylamide hydrogels with different surface structures," Friction 10, 360 (2020).

[18] J. Klein, "Shear, friction, and lubrication forces between polymer-bearing surfaces," Annu. Rev. Mater. Sci. 26, 581 (1996).

[19] K. Binder, T. Kreer, and A. Milchev, "Polymer brushes under flow and in other out-of-equilibrium conditions," Soft Matter 7, 7159 (2011).

[20] T. Kreer, "Polymer-brush lubrication: A review of recent theoretical advances," Soft Matter 12, 3479 (2016).

[21] M. Doi and S. F. Edwards, The Theory of Polymer Dynamics (Oxford University Press, 1988).

[22] T. C. O'Connor, N. J. Alvarez, and M. O. Robbins, "Relating chain conformations to extensional stress in entangled polymer melts," Phys. Rev. Lett. 121, 047801 (2018).

[23] P.-Y. Lai and K. Binder, "Grafted polymer layers under shear: A Monte Carlo simulation," J. Chem. Phys. 98, 2366 (1993).

[24] G. Peters and D. Tildesley, "Computer simulation of the rheology of grafted chains under shear," Phys. Rev. E 52, 1882 (1995).

[25] L. Miao, H. Guo, and M. J. Zuckermann, "Conformation of polymer brushes under shear: Chain tilting and stretching," Macromolecules 29, 2289 (1996).

[26] G. S. Grest, "Interfacial sliding of polymer brushes: A molecular dynamics simulation," Phys. Rev. Lett. 76, 4979 (1996).

[27] P. S. Doyle, E. S. Shaqfeh, and A. P. Gast, "Rheology of "wet" polymer brushes via Brownian dynamics simulation: Steady vs oscillatory shear," Phys. Rev. Lett. 78, 1182 (1997).

[28] P. S. Doyle, E. S. Shaqfeh, and A. P. Gast, "Rheology of polymer brushes: A Brownian dynamics study," Macromolecules 31, 5474 (1998).

[29] G. S. Grest, "Normal and shear forces between polymer brushes," in Polymers in Confined Environments, edited by S. Granick, K. Binder, P.-G. Gennes, E. P. Giannelis, G. S. Grest, H. Hervet, R. Krishnamoorti, L. Léger, E. Manias, E. Raphaël, and S.-Q. Wang (Springer, 1999), pp. 149–183.

[30] S. T. Milner, "Hydrodynamic penetration into parabolic brushes," Macromolecules 24, 3704 (1991).

[31] Y. Rabin and S. Alexander, "Stretching of grafted polymer layers," Europhys. Lett. 13, 49 (1990).

[32] M. Aubouy, J. Harden, and M. Cates, "Shear-induced deformation and desorption of grafted polymer layers," J. Phys. II 6, 969 (1996).

[33] F. Clément, T. Charitat, A. Johner, and J.-F. Joanny, "Self-assembled layers under flow: Stabilization by chain end exchange," Europhys. Lett. 54, 65 (2001).

[34] M. Müller and C. Pastorino, "Cyclic motion and inversion of surface flow direction in a dense polymer brush under shear," Europhys. Lett. 81, 28002 (2007).

[35] J. L. Barrat, "A possible mechanism for swelling of polymer brushes under shear," Macromolecules 25, 832 (1992).

[36] V. Kumaran, "Hydrodynamic interactions in flow past grafted polymers," Macromolecules 26, 2464 (1993).

[37] J. Harden and M. Cates, "Deformation of grafted polymer layers in strong shear flows," Phys. Rev. E 53, 3782 (1996).

[38] M. Rubinstein and R. H. Colby, Polymer Physics (Oxford University Press, 2003).

[39] A. Galuschko, L. Spirin, T. Kreer, A. Johner, C. Pastorino, J. Wittmer, and J. Baschnagel, "Frictional forces between strongly compressed, nonentangled polymer brushes: Molecular dynamics simulations and scaling theory," Langmuir 26, 6418 (2010).

[40] L. Spirin, A. Galuschko, T. Kreer, A. Johner, J. Baschnagel, and K. Binder, "Polymer-brush lubrication in the limit of strong compression," Eur. Phys. J. E 33, 307 (2010).

[41] J. Mees, R. Simič, T. C. O'Connor, N. D. Spencer, and L. Pastewka, "Molecular mechanisms of self-mated hydrogel friction," Tribol. Lett. 71, 74 (2023).

[42] K. Kremer and G. S. Grest, "Dynamics of entangled linear polymer melts: A molecular-dynamics simulation," J. Chem. Phys. 92, 5057 (1990).

[43] R. C. Armstrong, "Kinetic theory and rheology of dilute solutions of flexible macromolecules. I. Steady state behavior," J. Chem. Phys. 60, 724 (1974).

[44] G. S. Grest, "Computer simulations of shear and friction between polymer brushes," Curr. Opin. Colloid Interface Sci. 2, 271 (1997).

[45] G. S. Grest, Polymer brushes in strong shear flow, in Dynamics in Small Confining Systems III, Materials Research Society Proceedings (Cambridge University Press, 1996), Vol. 464, p. 71.

[46] S. De Beer and M. H. Müser, "Alternative dissipation mechanisms and the effect of the solvent in friction between polymer brushes on rough surfaces," Soft Matter 9, 7234 (2013).

[47] P. Espanol and P. Warren, "Statistical mechanics of dissipative particle dynamics," Europhys. Lett. 30, 191 (1995).

[48] P. J. Hoogerbrugge and J. M. V. A. Koelman, "Simulating microscopic hydrodynamic phenomena with dissipative particle dynamics," Europhys. Lett. 19, 155 (1992).

[49] W. M. de Vos and F. A. Leermakers, "Modeling the structure of a polydisperse polymer brush," Polymer 50, 305 (2009).

[50] M. K. Singh, P. Ilg, R. M. Espinosa-Marzal, M. Kröger, and N. D. Spencer, "Polymer brushes under shear: Molecular dynamics simulations compared to experiments," Langmuir 31, 4798 (2015).

[51] M. H. Müser, M. Urbakh, and M. O. Robbins, "Statistical mechanics of static and low-velocity kinetic friction," in Advances in Chemical Physics (John Wiley & Sons, Inc., 2003), Vol. 126.

[52] A. Schallamach, "The velocity and temperature dependence of rubber friction," Proc. Phys. Soc. B 66, 386 (1953).

[53] Y. B. Chernyak and A. I. Leonov, "On the theory of the adhesive friction of elastomers," Wear 108, 105 (1986).

[54] B. N. J. Persson, "On the theory of rubber friction," Surf. Sci. 401, 445 (1998).

[55] K. Vorvolakos and M. K. Chaudhury, "The effects of molecular weight and temperature on the kinetic friction of silicone rubbers," Langmuir 19, 6778 (2003).

[56] D. Maksuta, S. Dalvi, A. Gujrati, L. Pastewka, T. D. B. Jacobs, and A. Dhinojwala, "Dependence of adhesive friction on surface roughness and elastic modulus," Soft Matter 18, 5843 (2022).

[57] R. Faller, F. Müller-Plathe, and A. Heuer, "Local reorientation dynamics of semiflexible polymers in the melt," Macromolecules 33, 6602 (2000).

[58] P. Pincus, "Excluded volume effects and stretched polymer chains," Macromolecules 9, 386 (1976).

[59] S. Plimpton, "Fast parallel algorithms for short-range molecular dynamics," J. Comput. Phys. 117, 1 (1995).

[60] A. Stukowski, "Visualization and analysis of atomistic simulation data with OVITO–the open visualization tool," Modell. Simul. Mater. Sci. Eng. 18, 015012 (2009).